CrossMark

NOTE

The Jebel Ohier deposit—a newly discovered porphyry copper–gold system in the Neoproterozoic Arabian–Nubian Shield, Red Sea Hills, NE Sudan

F. P. Bierlein[1] · S. McKeag[2] · N. Reynolds[3] · C. J. Bargmann[2] · W. Bullen[1] · F. C. Murphy[3] · H. Al-Athbah[1] · C. Brauhart[3] · W. Potma[3] · S. Meffre[4] · S. McKnight[5]

Abstract Ongoing exploration in the Red Sea Hills of NE Sudan has led to the identification of a large alteration–mineralization system within a relatively undeformed Neoproterozoic intrusive–extrusive succession centered on Jebel Ohier. The style of mineralization, presence of an extensive stockwork vein network within a zoned potassic-propylitic-argillic-advanced argillic-altered system, a mineralization assemblage comprising magnetite-pyrite-chalcopyrite-bornite (±gold, silver and tellurides), and the recurrence of fertile mafic to intermediate magmatism in a developing convergent plate setting all point to a porphyry copper–gold association, analogous to major porphyry Cu–Au–Mo deposits in Phanerozoic supra-subduction settings such as the SW Pacific. Preliminary U–Pb age dating yielded a maximum constraint of $c.$ 730 Ma for the emplacement of the stockwork system into a significantly older ($c.$ 800 Ma) volcanic edifice. The mineralization formed prior to regional deformation and accretion of the host terrane to a stable continental margin at by $c.$ 700 Ma, thus ensuring preservation of the deposit. The Jebel Ohier deposit is interpreted as a relatively well-preserved, rare example of a Neoproterozoic porphyry Cu–Au system and the first porphyry Cu–Au deposit to be identified in the Arabian–Nubian Shield.

Keywords Porphyry Cu–Au · Neoproterozoic · Red Sea Hills · U–Pb age dating · Arabian–Nubian Shield

Editorial handling: H. Frimmel

✉ F. P. Bierlein
   fbierlein@qatarmining.com

[1] Qatar Mining, PO Box 20405, West Bay, Doha, Qatar

[2] QMSD Mining Co Ltd, PO Box 7828, Khartoum, Sudan

[3] CSA Global Pty Ltd, PO Box 141, West Perth, WA 6872, Australia

[4] ARC Centre of Excellence in Ore Deposits, University of Tasmania, Hobart, TAS 7001, Australia

[5] School of Science and Engineering, Federation University, P.O. Box 663, Ballarat, Victoria 3353, Australia

Introduction

Recent and ongoing exploration work by Qatar Mining Sudan Co Ltd ("QMSD") on its Block 62 exploration concession in the Red Sea Hills of NE Sudan (Fig. 1) has delineated an extensive Cu–Au-dominated stockwork mineralization associated with an outward-zoned potassic-propylitic-argillic-advanced argillic alteration system in a multi-phase Neoproterozoic intrusive-extrusive igneous succession. The mineralized system is centered on a topographic high named "Jebel Ohier" by the local Beja tribe. The system is quite distinct from previously recognized mineralization in the Red Sea Hills in Sudan, namely orogenic gold mineralization that has supported extensive historical gold mining activity since Pharaonic times (Klemm et al. 2001) and which is currently the source of the bulk of Sudan's gold production (mainly through extensive artisanal mining; Geological Research Authority of Sudan, written commun. 2015). The Jebel Ohier deposit is also dissimilar from well-documented Cu–Zn–Au VHMS (volcanic-hosted massive sulfide) mineralization as exemplified by the deposits of the Ariab district (e.g., Cottard et al. 1986).
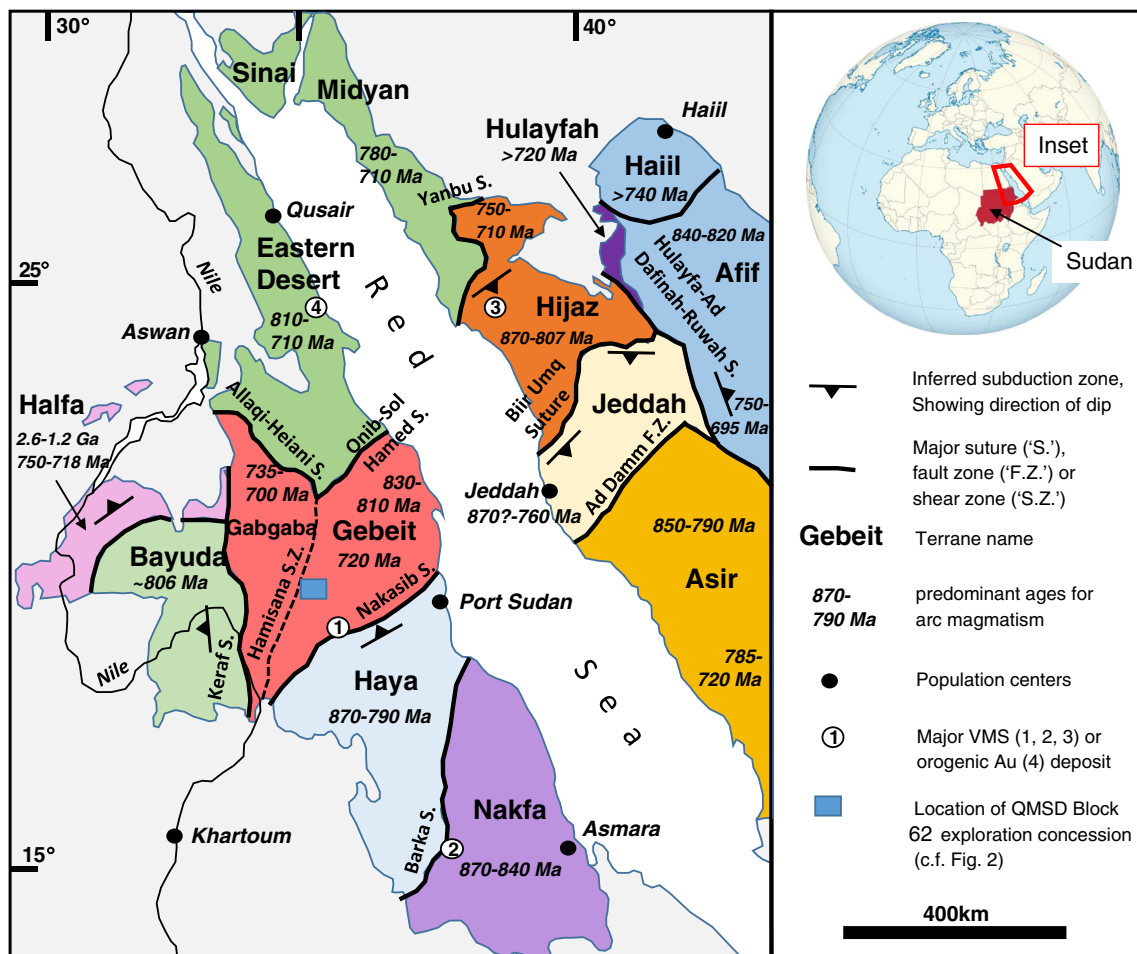
Fig. 1 Terranes and sutures of the Arabian–Nubian Shield showing predominant ages for arc magmatism in each terrane (from Kröner and Stern 2005), as well as the location of QMSD's Block 62 exploration concession (c.f. Fig. 2), major structural elements, principal localities and principal mines (*1* Ariab, *2* Bisha, *3* Jebel Sayid, *4* Sukari)

The Jebel Ohier mineralized system is situated in a remote desert region some 300 km to the west-northwest of Port Sudan (Fig. 1) and was first documented during reconnaissance fieldwork carried out by Bureau de Recherches Géologiques et Minières (BRGM) in the early 1980s as part of the regional exploration program that located the Ariab deposits (Cottard et al. 1986). Later, Anglo American Corporation geologists, following up on the BRGM work, also visited Jebel Ohier in 1995 ((Surtees et al. (2012) Review of concessions and mineral potential of Sudan. Report for Qatar Mining, unpublished). The Geological Research Authority of Sudan (GRAS) conducted a regional geochemical sampling program as well as grid soil and rock-chip sampling at the Jebel Ohier prospect in 2004 and 2005 (Adde 2004, 2005).

No systematic modern-day exploration had been undertaken in the study area prior to the granting of an exploration lease to QMSD in 2013, and the nature and origin of the mineralized system remained undetermined. Geochemical sampling and prospect mapping was followed by a preliminary 5600 m RC drilling program between September 2014 and February 2015. Together with extensive trench and channel sampling, the program has confirmed the presence of a large Cu–Au system at Jebel Ohier, with wide zones of mineralization, grading between 0.2 and 1.5 wt% Cu, developed in the 35 to 75 m thick (from surface) oxide zone of the system. Broad drill intervals of >0.5 wt% Cu and up to 0.45 g/t Au have been intercepted repeatedly from below the base of the oxide zone to 200 m depth. The system remains open laterally and at depth. A resource estimate has not been calculated yet.

This study documents some geologic, petrographic, and geochronologic features of what is interpreted to be the first porphyry copper deposit (PCD) identified in the Neoproterozoic Arabian–Nubian Shield (ANS) in NE Africa, a geologically complex region with demonstrated pedigree for world-class orogenic gold (e.g., Sukari) and gold-rich polymetallic volcanic-hosted sulfide deposits (e.g., Ariab, Bisha, and Jebel Sayid; Fig. 1), but hitherto considered

to have extremely low potential for the preservation of porphyry Cu systems.

Regional geology

The ANS is an accretionary orogenic belt comprising a series of predominantly juvenile intra-oceanic island arcs, oceanic islands and micro-continental masses which extends along both sides of the Red Sea from Egypt in the NW, the Sinai Peninsula in the N, and Saudi Arabia in the NE, to Ethiopia and Yemen in the SW and SE, respectively (Johnson et al. 2011). The ANS evolved between 900 and 550 Ma in response to the closure of the Mozambique Ocean (800–650 Ma) and the subsequent collision between East and West Gondwana (Stern 1994, 2002). The Red Sea Hills constitute the Sudanese and Egyptian parts of the ANS.

Kröner et al. (1987) divided the Red Sea Hills area into geologically distinct crustal segments (terranes) that are separated from each other by ophiolite-decorated suture zones. The study area (QMSD's "Block 62" exploration concession) lies within the Gebeit Terrane (Reischmann and Kröner 1994; Fig. 1) which comprises arc-related low-grade volcano-sedimentary sequences and syn-tectonic igneous complexes in the area to the north of the Nakasib Suture (Klemenic 1985; Vail 1985). Whole rock Rb-Sr isochron ages around 720 Ma were reported for volcanic and plutonic rocks from the terrane by Fitches et al. (1983) and Almond and Ahmed (1987), with somewhat older ages of about 830 Ma obtained by Reischmann (1986; unpublished PhD thesis cited in Reischmann and Kröner 1994) for volcanic rocks elsewhere in the Gebeit Terrane using Sm–Nd dating methods. The Nakasib Suture is a *ca.* 150 km-long NE-trending fold and thrust belt in the central part of the Red Sea Hills and formed as a result of collision between the Haya and Gebeit terranes at *ca.* 750 Ma (Abdelsalam and Stern 1993). The Nappe emplacement from north to south (Adbelsalam 2010) suggests that closure was by northward subduction beneath the Gebeit Terrane. Collision of the composite Haya/Gebeit Terrane with the Sahara Metacraton across the Keraf Suture occurred ca. 650–580 Ma culminating in final collision with the Arabian plate. Post-accretion compressional and extensional deformation zones within the Gebeit and adjacent terranes was manifested by major shear zones and non-orthogonal wrench faults such as the NW–SE trending Najd system, the N–S trending Hamisana Shear Zone (HSZ), and the Oko Shear Zone (Abdelsalam 2010; Fig. 1).

Geology of the Jebel Ohier mineral system

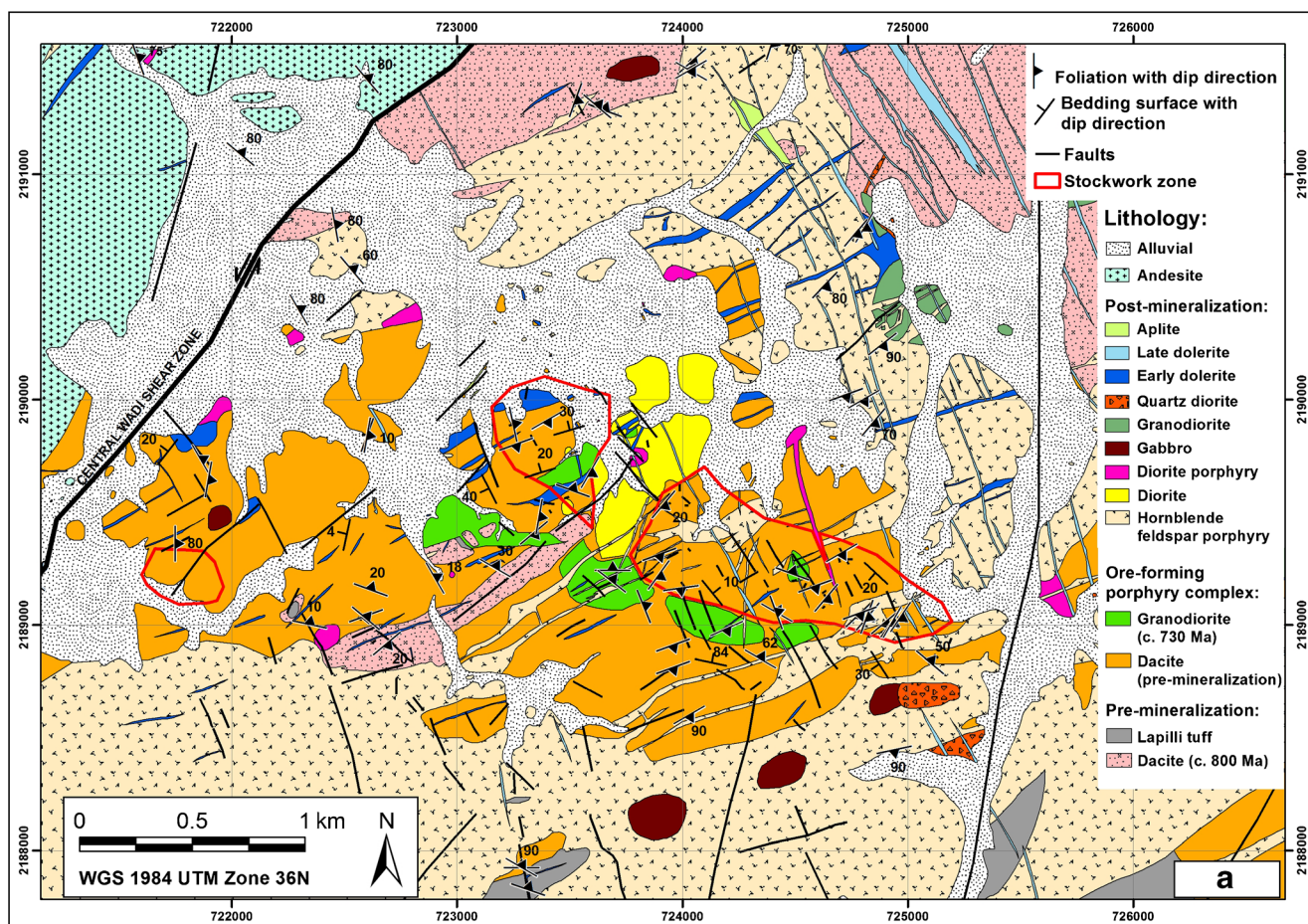In the Jebel Ohier prospect area, the geology is characterized by volcano-intrusive units which range in composition from (sub-alkaline) gabbroic to granodioritic-dacitic. This ore-forming porphyry complex was emplaced into an older (pre-mineralization) andesitic to dacitic, and in places tuffaceous volcanic sequence. The mineralization and alteration system itself occurs in a thick massive to laminated dacitic unit (Figs. 2 and 3a–c) in the NE of the alteration zone. These dacitic volcanic rocks were intruded by a co-magmatic granodiorite (Figs. 2 and 3a) with a "crowded" feldspar-hornblende porphyritic texture. A distinct (post-mineralization) porphyritic intrusive suite, termed "hornblende feldspar porphyry", as well as a series of (post-mineralization) intermediate to mafic intrusive plugs, stocks and dykes, were emplaced within the dacite and granodiorite (Fig. 3d–f).

Andesitic ashfall tuffs and volcaniclastic agglomerates were observed some 5 km to the south of the deposit. In contrast to other parts of the Gebeit Terrane (e.g., Reischmann and Kröner 1994), clastic sedimentary rock types are virtually absent from the Jebel Ohier area. A belt of andesitic rocks to the west of Jebel Ohier (Fig. 2a) includes massive volcanic rocks and tuffs as well as epiclastic andesitic sandstones and local limestone. The temporal relationship between the andesitic belt and the intrusive-extrusive system at Jebel Ohier remains undetermined. Further (*ca.* 20 km) to the south and southwest, mudstones with mud cracks, alluvial cobble conglomerates and siltstones, indicative of a sub-aerial depositional environment, have been mapped as overlying the andesitic volcanic rocks and epiclastic sedimentary rocks. There is no evidence of deep water sedimentary rocks anywhere in the study area, suggesting that Jebel Ohier reflects a shallow-marine to emergent setting, with a significant portion of the sub-aerial component of the succession possibly having been eroded in response to tectonic uplift.

Metamorphism in the study area is generally of low-grade (greenschist facies), as indicated by the occurrence of actinolite, chlorite, epidote, and clinozoisite in andesitic rocks. In the vicinity of batholithic intrusions and within prominent N–S shear zones on the eastern margin of the Jebel Ohier block, metamorphism increases up to amphibolite facies, with incipient leucosome development within andesitic units observed in some places.

Structural framework

Bedding in the volcanic sequence at Jebel Ohier shows shallow to moderate dips of variable but predominantly northerly orientation (Fig. 2a). The regional D1 deformation is the principal fabric-forming event; S1 ranges from entirely absent in competent intrusive units to spaced or penetrative in strongly altered and fine-grained volcanic assemblages. D1 strain is localized strain along a major NE-trending sinistral shear zone W of Jebel Ohier prospect called the Central Wadi Shear Zone (Fig. 2). The S1 fabric rotates from a NE to ENE trend through

Fig. 2 **a** Simplified geological map of the Jebel Ohier area showing major rock units, structural trends, and extent of the stockwork zone. **b** Extent and orientation of major alteration zones mapped at Jebel Ohier

the prospect area, interpreted to reflect later D2 rotation accompanying large-scale open folding. The latest phases of deformation are documented by weak open folds, local kinks, and brittle deformation associated with NW–SE and east–west striking faults. Several N–S and sets of NW- and NE-trending faults cut the prospect area.

Sequence of volcanic and intrusive rocks

The mineralized stockwork and associated alteration pre-date—but are only weakly affected by—all recognized deformation events. Importantly, the stockwork zone appears relatively intact with only minor displacement evident on late-stage faults. In addition to plug- and stock-like intrusions post-dating the mineralization, several sets of overprinting dykes are also present. These vary in composition from dioritic to granodioritic and gabbroic, with textures ranging from porphyritic to medium- and fine-grained doleritic. Temporal relationships vary from pre- to post-stockwork, and from pre- to post-deformation, with NNW–SSE trending dolerite dykes representing the youngest swarms (Fig 2; note that the

exposure of pre-mineralization dykes is limited to a few outcrops; these cannot be visualized in Fig. 2a). Broadly, the concentration of intrusive rocks in the prospect area and the overlap of dyke sets with stockwork veining provide strong evidence that the mineralization is related to a multi-stage porphyritic magmatic event culminating in the post-stockwork hornblende feldspar porphyry. A switch in principal stress orientation during the evolution of the system is inferred from broadly orthogonally orientated dyke swarms. A laterally extensive post-mineralization diorite body cuts the stockwork system in the western part of the mineralized zone, effectively demarcating a western and an eastern stockwork zone (Fig. 2).

Alteration

The ca. 2.0 by 0.5 km wide stockwork zone, which defines the core of the ca. 4.0 by 1.4 km wide alteration system at Jebel Ohier, is dominated by pervasively quartz-sericite-chlorite altered and in places strongly silicified (±pyrite bearing) dacite and granodiorite (Fig. 2a, b). To the south and west, the altered
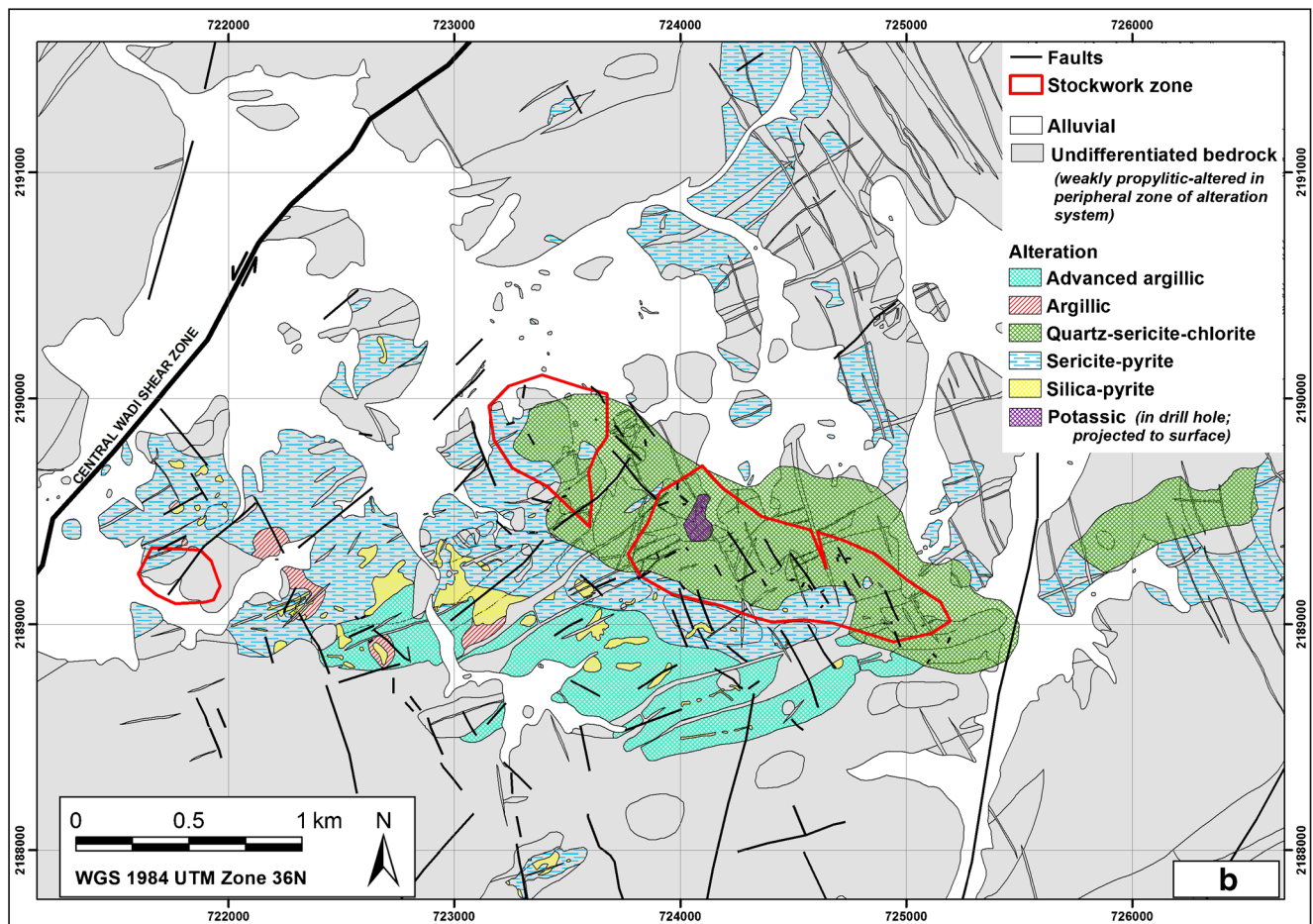
Fig. 2 continued.

stockwork passes via phyllic sericite±pyrite-dominated alteration into an extensive area of strong, pervasive kaolin development and intense bleaching. This bleached zone is inferred to represent the lithocap of the hydrothermal system. The argillic alteration encompasses zones of advanced argillic alteration with a quartz-andalusite-pyrophyllite assemblage and pervasively silicified tuff beds (Arne et al. 2014). This alteration zone is abruptly truncated to the south by the post-mineralization hornblende feldspar porphyry, although minor alteration also occurs south of this intrusion. To the north, the stockwork zone is bounded by a weaker and less pervasive phyllic sericite±pyrite alteration zone without stockwork vein development. The peripheral zones of the hydrothermal system are characterized by weakly developed propylitic epidote-carbonate-chlorite alteration in andesite. Potassic alteration has been locally observed (Fig. 3f) in outcrop and drill chips from within the stockworked zone but not at the scale of the exposed system. The overall geometry of the hydrothermal alteration currently exposed at Jebel Ohier suggests that the core of the system, and with it the center of the potassic alteration, might occur at depth and to the northeast of Jebel Ohier.

Mineralization style

The stockwork zone in the Jebel Ohier system comprises vein styles ranging from thin (1–25 mm across), veinlets to thicker (20–100 mm across), more laterally continuous, laminated to massive veins, asymmetric veins, and irregular-shaped, thin to massive veins (Fig. 3g, h). The veinlets, which are interpreted to represent "A" veins in the classification scheme of Gustafson and Hunt (1975), are typically discontinuous and erratically orientated (in early feldspar-hornblende porphyries) to re-aligned/flattened (in tuffaceous dacite) and contain rare sulfides. Interpreted "B" veins tend to occur in the form of low-angle sheets within dacite and, to a lesser extent, in pre-mineralization feldspar-hornblende porphyry. The larger B veins cut across A veinlets, display elongate quartz textures perpendicular to planar vein walls and, in examined sections from the hypogene zone, typically contain characteristic sulfide—Fe-oxide—carbonate central domains and narrow sericitic selvages. In an outcrop, B veins are commonly coated by a variably thick layer of chrysocolla with minor malachite, and there appears to be a positive correlation between Cu–Au

Fig. 3 **a** Argillic-altered dacite with disseminated boxwork textures. **b** Syn-mineralization feldspar-hornblende granodiorite with minor stockwork development (sample FBJO-043, dated at *ca.* 730 Ma). **c** Exposure of *ca.* 800 Ma tuffaceous dacite raft (*outlines* indicated by *polygon*; *ca.* 4 m in length) with flattening fabric within massive syn-mineralization granodiorite. **d** Normal fault contact of stockwork-hosting dacite and post-mineralization hornblende feldspar porphyry. **e** Late, un-foliated dyke cutting early, altered foliated dyke and stockworked dacite. **f** Potassic alteration (pink K-feldspar partially seriticized; hydrothermal biotite partially replaced by chlorite) associated with stockwork veinlet selvages in hand specimen from syn-mineralization granodiorite. **g** Exposure of intensively stockworked, propylitic-altered dacite. **h** Example of a massive interpreted B vein with the *center line* cutting across interpreted A veinlets in dacite
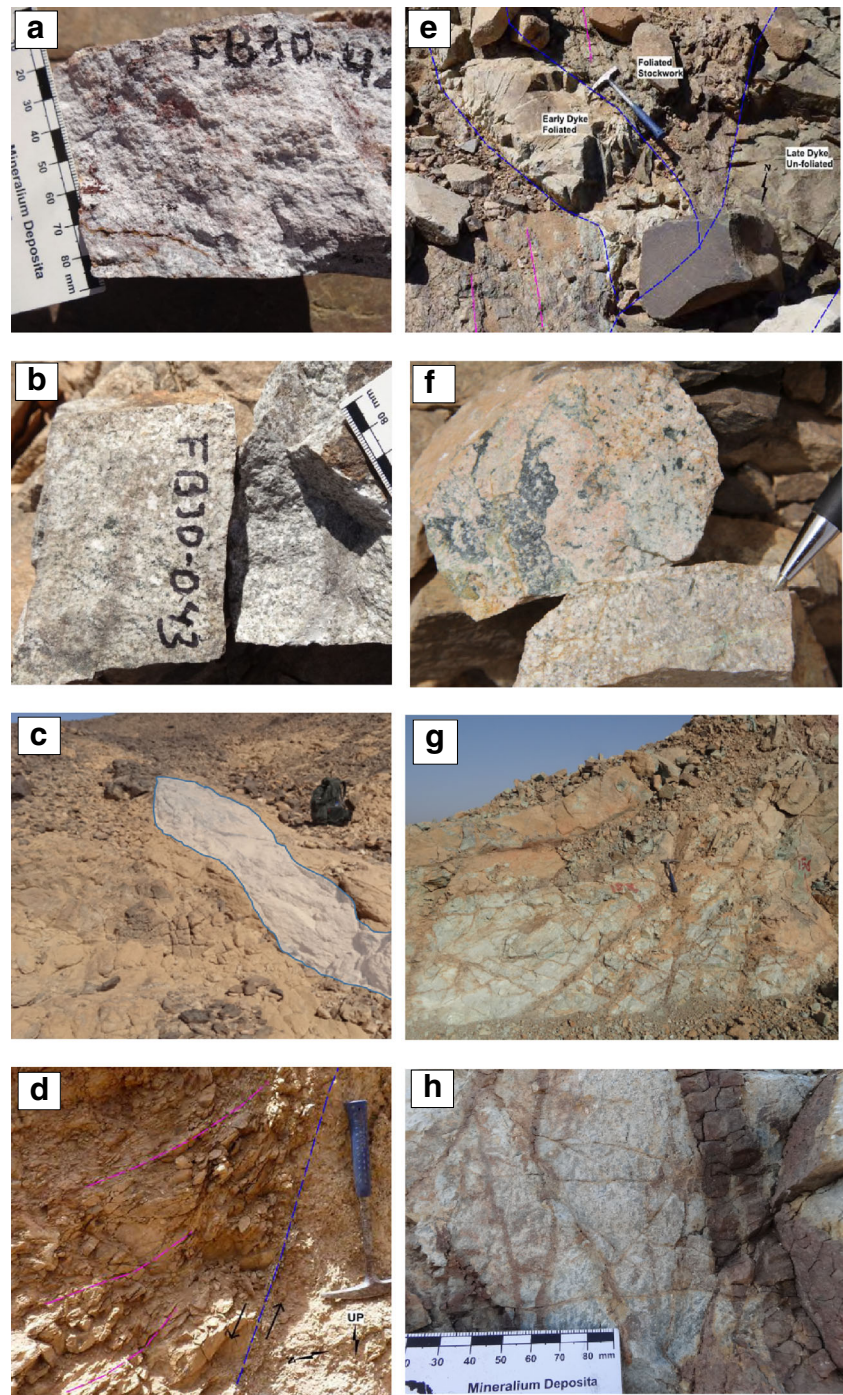
grades and the abundance and intensity of stockworking. Linear to warped, up to 5 cm thick quartz-magnetite-sulfide ±actinolite veins (possible "M" veins; e.g., Sillitoe 2010) are almost entirely developed within the dacite and are characterized in outcrop by a high abundance of Fe-oxides lining the vein walls as well as forming irregular masses within vein centers. In addition, the mineralized zone hosts rare 0.5 to 1 m wide, massive to semi-planar veins that are characterized by re-crystallized to brecciated quartz, subordinate K-feldspar, boxwork after sulfides, and irregular Fe-oxide aggregates. These veins generally cut across the earlier stockwork veins and are associated with <20 cm-wide sericite-carbonate-bleached wallrock selvages.

Other than stockwork-related examples, there is a relative paucity of quartz veins exposed in the Jebel Ohier area. This in itself is remarkable given the degree of deformation and

rheological contrasts, and suggests a lack of fluid over-pressuring during deformation (e.g., Sibson 2001). Although further detailed study will be required, overall the vein patterns and distinctive sequence of stockwork development at Jebel Ohier closely resemble those widely described from many productive porphyry Cu–Au deposits such as El Salvador, Ok Tedi and Grasberg (e.g., Gustafson and Hunt 1975; Sillitoe 2000, 2010).

Ore paragenesis

Polished mounts of sulfide-bearing RC drill chips were prepared, with SEM work carried out using a JEOL^{TM} JSM 6300 SEM at Federation University (Ballarat, Australia) to identify the ore phases (Fig. 4), constrain the paragenetic sequence of mineralization (Fig. 5), and determine the siting of gold in the mineralized samples. Backscattered electron images (BSE) and energy dispersive X-ray spectroscopy (EDS) data were acquired using an Oxford Instruments Link Analytical System. Electron beam conditions were 15 kV and 1.5 nA for BSE imagery, and 15 kV and 5 nA for quantitative EDS analysis. At these beam current conditions, the calculated detection limit for gold in chalcopyrite is about 2000 ppm.

The main sulfide phases at Jebel Ohier are pyrite and chalcopyrite which occur both as disseminated phases and in B/D veins (Fig. 4a–g). Chalcopyrite typically fringes and penetrates pyrite grains along fractures (Fig. 4b). Quantitative EDS analysis confirmed a lack of geochemical zonation (i.e., Cu, Fe) in pyrite and chalcopyrite. Low-Fe sphalerite (1.5–6 wt% Fe), galena and bornite, and rare pyrrhotite (as small inclusions in pyrite porphyroblasts) occur as subordinate phases in stockwork veins and rarely as disseminated grains in pervasively silicified dacite. Magnetite represents an early hydrothermal phase in disseminated form within more mafic-intermediate host rocks, as well as associated with pyrite and chalcopyrite in quartz-magnetite-sulfide±actinolite veins (Fig. 4a). Where affected by supergene overprint, the Fe-oxide is commonly altered to martite and/or ilmenite. Bornite in these instances is replaced by covellite and/or chalcocite (Fig. 4c). Gold has been observed (though exceedingly rarely due to the available sample medium) as minute visible grains in vein quartz and feldspar, and within cracks of the principal sulfides in possible B veins (Fig. 4d, e). There is no visual or analytical evidence that gold occurs in solid solution or as a refractory phase in pyrite or chalcopyrite. The ore assemblage and low-Fe content of the sphalerite provides a rough upper estimate of c. 400 to 450 °C for ZnS formation at Jebel Ohier (based on Scott 1983).

Molybdenite laths can be observed as inclusions in large (>4 mm across) pyrite aggregates in some vein-hosting samples (Fig. 4g). Additional accessory phases—almost ubiquitous in all samples but typically as sub-50 micron grains

within fractures in, or attached to the rims of the main sulfides in B veins—comprise empressite-hessite, sylvanite, altaite, and enargite. The presence and texturally late association of these phases, in conjunction with the nature of liquid-vapor-solid (LVS) and vapor-rich fluid inclusions observed in B-vein quartz (Fig. 4h), suggest their precipitation occurred under progressively lower hydrothermal temperature conditions (cf. Fig. 5) from a moderately to hyper-saline fluid (e.g., Bodnar 1995; Sun et al. 2013).

U–Pb geochronology

Representative off-cuts from three igneous samples (FBJO-001, -043 and -044) were crushed and non-magnetic heavy minerals separated at the Australian Research Council Centre of Excellence in Ore Deposits (CODES) at the University of Tasmania (Hobart, Australia) using gravity and magnetic separation techniques. The heavy mineral concentrate from each of the three samples was mounted in 25 mm epoxy blocks and polished to expose the zircon crystals. The zircons were then analyzed on an Agilent 7900 quadrupole ICP-MS with a 193 nm Coherent Ar–F gas laser and the Resonetics S155 ablation cell at the University of Tasmania using similar techniques to that outlined in Halpin et al. (2014).

A mineral separate containing zircon, pyrite, and apatite from a syn-mineralization feldspar-hornblende granodiorite with cubic boxwork and hosting A, B, and quartz-magnetite-sulfide veins (sample FBJO-043; cf. Fig. 3b) yielded numerous large euhedral zircon grains ranging from 50–150 μm in length. Of these, 29 zircon grains were selected and analyzed, all giving a ^{207}Pb-^{206}Pb age of 732±7 (2σ) Ma (Cryogenian) within the analytical uncertainty of each other (Fig. 6a). All of the zircon grains analyzed are concordant or close to concordant on the Tera-Wasserburg and Wetherill Concordia diagrams (Fig. 6 and Table 1), however, the trend of the data suggests that a small amount of Pb loss has occurred. Lead loss does not affect the ^{207}Pb-^{206}Pb age which was used to estimate the age of the rock. The zircon grains have moderate U and relatively low Ti contents and typical magmatic U–Th ratios.

The zircon grains from a dacitic pre-mineralization tuff without stockwork veining (sample FBJO-044) are larger than those in FBJO-043 (50–250 μm) and tend to be more rounded suggesting resorption (Fig. 6b). The majority of the grains analyzed have a ^{207}Pb corrected ^{206}Pb/^{238}U age of 806± 7 Ma (2σ) with 3 crystals showing older ages interpreted as inherited crystals (Fig. 6b). A ^{207}Pb corrected age was used in this sample and FBJO-001, as a small amount of common Pb was detected in some of the grains. The ^{207}Pb-^{206}Pb age is very similar to the ^{207}Pb corrected ^{206}Pb-^{238}U age of 809± 26 Ma excluding both the older grains and one grain with

Fig. 4 a Reflected light photomicrograph of magnetite (*mt*)–pyrite (*py*)–chalcopyrite (*cp*) in a quartz-magnetite-sulfide vein. **b** Reflected light photomicrograph showing pyrite (*py*) overgrown by chalcopyrite (*cp*) in the B vein. **c** Reflected light photomicrograph showing B vein pyrite (*py*) containing enargite (*en*) inclusion and intergrown with chalcopyrite (*cp*); cp partially replaced by covellite (*co*). **d** Reflected light photomicrograph showing disseminated gold (*Au*) inclusion in quartz, near chalcopyrite (*cp*). **e** Reflected light photomicrograph of B vein chalcopyrite (*cp*) stringer intergrown with pyrite (*py*), magnetite (*mt*), and sphalerite (*sp*); cp containing empressite (*em*) and gold (*Au*) inclusions; cp overgrown by bornite (*bn*), bn partially replaced by covellite (*co*). **f** Backscattered electron image of galena (*ga*) stringers filling cracks within pyrite (*py*) granoblast in B vein; py intergrown with chalcopyrite. **g** Molybdenite (*mo*) lath in pyrite (*py*) granoblast (*cp*) and sphalerite (*sp*). **h** Transmitted light photomicrograph showing liquid-vapor-solid (*L-V-S*) and aqueous liquid-vapor (*L-V*) fluid inclusions in B vein quartz hosting pyrite-chalcopyrite assemblage
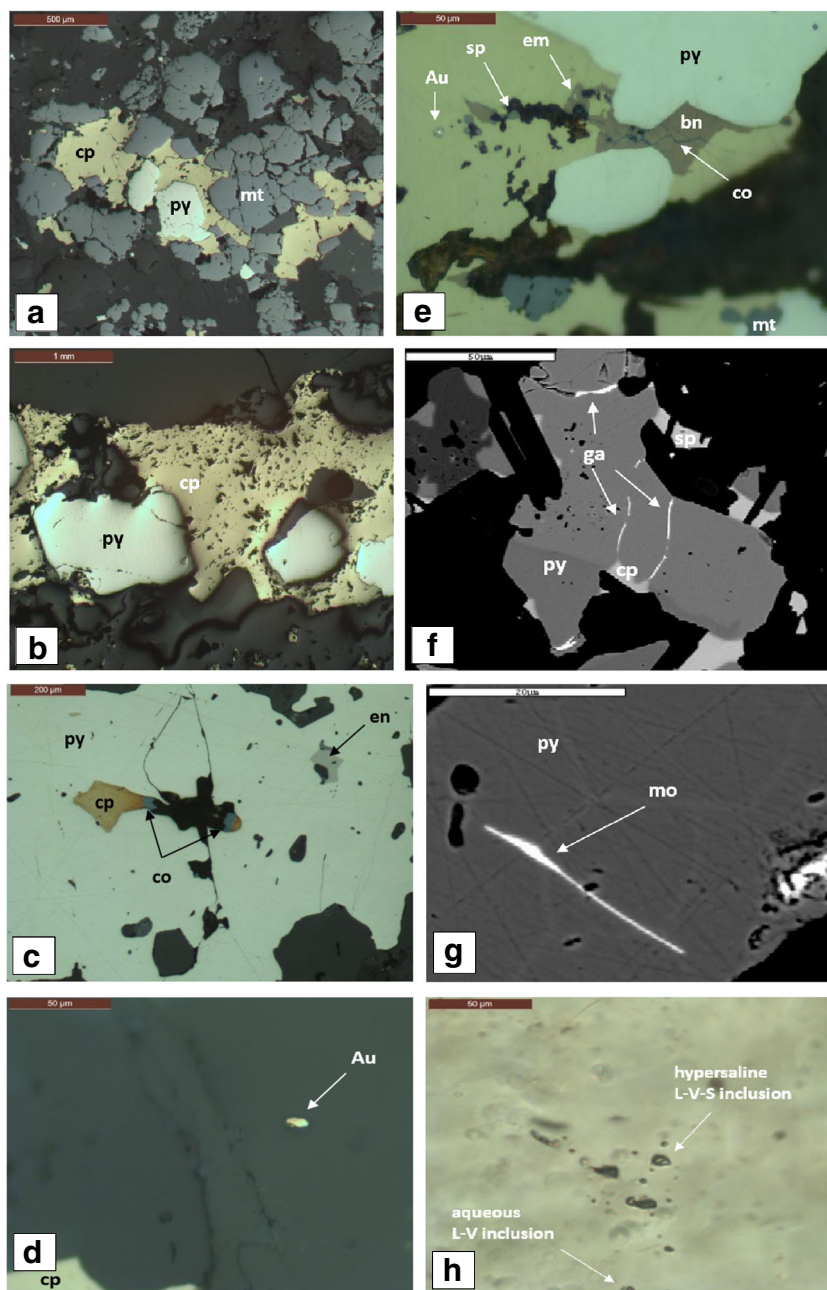
common Pb. The zircon grains have low U and relatively low Ti contents and typical magmatic U–Th ratios (Table 1).

The zircon grains in sample FBJO-001, a stockwork-hosting syn-mineralization granodiorite porphyry are much smaller (20-50 μm) and are rarer than in the previous sample, with both rounded and euhedral zircon grains present (Fig. 6c). The ^{207}Pb-^{206}Pb age is slightly older but within the analytical uncertainty to the ^{207}Pb corrected ^{206}Pb-^{238}U age of 745±19 Ma excluding both the older grains and two grains with common Pb. The majority of the crystals analyzed have a

^{207}Pb corrected ^{206}Pb-^{238}U age of 727±7 Ma (2σ) with 3 grains showing older ages interpreted as inherited crystals (Fig. 6c). The zircon grains have moderate U and relatively low Ti contents and typical magmatic U–Th ratios (Table 1).

Discussion

Based on the geological, textural, structural, petrographic, and geochronologic evidence described herein, the mineralization

Fig. 5 inferred paragenetic sequence of ore-forming sulfide and oxide phases at Jebel Ohier against temperature and time (*time and temperature axes* not to scale)

Paragenetic sequence
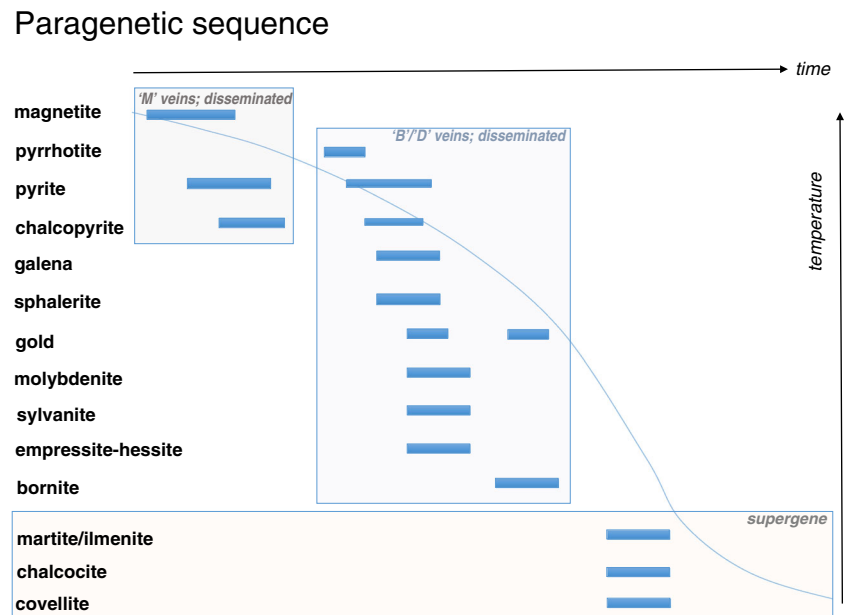
system at Jebel Ohier is interpreted as a relatively well-preserved example of a Neoproterozoic Cu–Au porphyry system associated with an ancient convergent plate boundary in the Arabian–Nubian Shield. The U–Pb ages obtained for three igneous samples from the Jebel Ohier system provide a well-constrained maximum age of about 730 Ma for porphyry Cu–Au mineralization. Although a minimum constraint is as yet lacking (samples from two post-stockwork intrusions have yielded insufficient zircons), the development of the stockwork system pre-dates regional deformation and suturing of the Gebeit and Haya terranes in the ANS at or before 700 Ma (Abdelsalam 2010) by up to 30 m.y. The *c*. 800 Ma age constraint for the barren (pre-mineralization) dacitic tuff implies that the magmatic-mineralizing event(s) was/were preceded by a significantly older phase of intermediate to felsic volcano-intrusive activity.

The petrological and textural characteristics of the volcanic-intrusive complex demonstrates that the younger magmatic event that drove the porphyry-style Cu–Au mineralization was associated with the injection of more mafic to intermediate, hornblende-rich material. The rise of this ore-forming magmatic pulse may have been related to a specific tectonic event late in the evolution of the arc, as is common in many porphyry districts (Richards et al. 2001; Vos et al. 2007; Richards 2009; John et al. 2010 and references therein; Sillitoe 2010).

The preservation of relatively gently inclined layering or enveloping surfaces in the dacitic volcanic pile at Jebel Ohier suggests that the paleo-horizontal is close to current topography, rather than being tilted steeply on end, overturned or dismembered. The existence of lithocap facies and general lack of high-temperature alteration is taken to indicate that the porphyry which generated the stockwork may still be preserved at relatively shallow depth beneath the mineralized zone.

The overwhelming majority of PCDs globally are Mesozoic to Cenozoic in age and occur mainly in the circum-Pacific, Tethys–Himalaya, and Central Asia metallogenic belts (Garwin et al. 2005; Seedorff et al. 2005; John et al. 2010). This distribution pattern along geologically relatively young plate margin settings is because PCDs and their genetically linked high- and low-sulfidation epithermal Au–Ag deposits form at shallow crustal levels in arc and back-arc settings that are characterized by high uplift rates (e.g., Kesler and Wilkinson 2006). These evolving geological settings have a high susceptibility to erosion and, in turn, determine the relatively poor preservation potential of PCDs. Consequently, PCDs are most abundant in Mesozoic and Tertiary terranes (e.g., Groves et al. 2005; Kesler and Wilkinson 2006), rare in Paleozoic terranes (e.g., the porphyry Cu–Au deposits of eastern Australia and the Altaid orogenic collage; Walshe et al. 1995; Yakubchuk et al. 2005; Wu et al. 2015), and are very rare in older terranes. The few documented examples of Precambrian porphyry deposits include those in the Dharwar Craton of central India (e.g., Stein et al. 2004), the Fennoscandian Shield (Gaál and Isohanni 1979; Beigarn et al. 2013), the Pilbara Craton (e.g., Barley 1982), in Namibia (Malenda et al. 2014), in the Superior province of Quebec (Goodman et al. 2005), the Goiás Magmatic Arc in central Brazil (de Oliveira et al. 2015), and possibly at Boddington in the Yilgarn Craton of Western Australia (Qui and Groves 1999). In all instances, the preservation of these ancient PCDs can be linked to selective protection from subsequent uplift and excessive erosion due to accretion of the hosting arcs to stable continental blocks not long after their formation (Bierlein et al. 2009). The timing of mineralization at Jebel

Fig. 6 Reflected light microscope photos showing zircon crystals separated from samples (**a**) FBJO-043, (**b**) FBJO-044, and (**c**) FBJO-01 and spots analyzed (*blue dots*), and Wetherill Concordia diagram showing the isotopic composition of the zircons in each of the samples. The ages, regressions, and mean square weighted deviations shown in these diagrams were calculated using the Isoplot software (Ludwig 2012). The age shown in concordia diagram (**a**) is an upper intercept based on regression of all of the data shown in the *red ellipses*. The ages on concordia diagrams in (**b**) and (**c**) are lower intercepts on concordia with the upper intercept anchored to the common Pb composition predicted by the model of Stacey and Kramers (1975) at 806 and 727 Ma, respectively
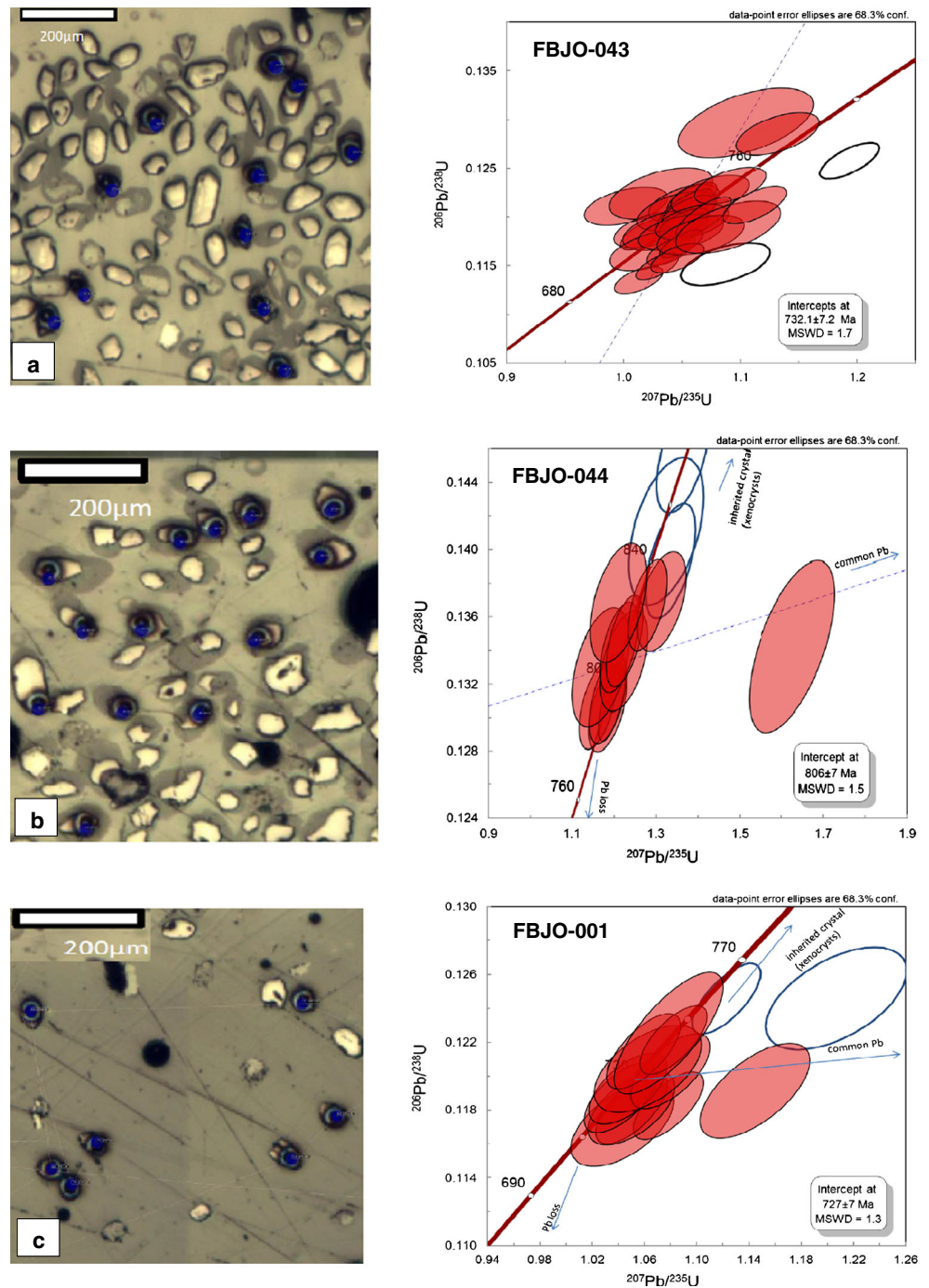
Ohier, when viewed in the context of the tectonic evolution of the ANS, strongly suggests that this serendipitous conjunction of tectonic events in space and time (i.e., intra-oceanic arc formation, injection of fertile asthenospheric melt, rapid accretion to established continental margin) played a critical role in the formation and preservation of the Jebel Ohier porphyry Cu–Au system. The association of Precambrian porphyry Cu–Au–Mo deposits with calc–alkaline basalt–andesite–dacite–rhyolite rocks that dominate Phanerozoic accretionary orogens suggests that the key ore-forming tectono-magmatic processes changed little over time (Kerrich et al. 2005).

Conclusions

Ongoing exploration (including diamond drilling, airborne and ground-based geophysical surveys, metallurgical studies, etc.) and continuous assessment of the Jebel Ohier

mineralized system in due course will allow for a more comprehensive understanding of the deposit's origin, its economic potential, and why it has been preserved so well. However, the evidence gathered so far provides a firm basis for the interpretation of Jebel Ohier as a rare example of a Neoproterozoic porphyry Cu–Au deposit. Evidence in support of this notion include the (i) nature of the host rocks and multi-phase porphyritic intrusive succession; (ii) style and zonation of hydrothermal alteration and mineralization; (iii) presence of a distinctive stockwork veining system with interpreted A, B, and quartz-magnetite-sulfide±actinolite veins; (iv) overall grade and distribution of Cu and Au within a large volume of (sub-) alkaline volcano-intrusive rocks; (v) mineral assemblage and paragenetic sequence, and (vi) the *c.* 730 Ma age constraint for mineralization. Jebel Ohier also represents the first porphyry Cu–Au deposit identified in the Neoproterozoic Arabian–Nubian Shield. The discovery of porphyry-style Cu–Au mineralization in a Precambrian region previously considered not prospective for this deposit style demonstrates once more the importance of continuously challenging existing exploration paradigms and to "expect the unexpected".

References

Abdelsalam MG (2010) Quantifying 3D post-accretionary tectonic strain in the Arabian–Nubian Shield: superimposition of the Oko Shear Zone on the Nakasib Suture, Red Sea Hills, Sudan. J Afr Earth Sci 56:167–178

Abdelsalam MG, Stern RJ (1993) Structure of the late Proterozoic Nakasib suture, Sudan. J Geol Soc Lond 150:1065–1074

Adde AE (2004) Preliminary geochemical gold exploration at Jebel Oheir Area, NE Sudan, GRAS, Sudan (unpublished)

Adde AE (2005) Phase 2 geochemical gold exploration at Jebel Oheir Area, NE Sudan, GRAS, Sudan (unpublished)

Almond DC, Ahmed F (1987) Ductile shear zones in the northern Red Sea Hills, Sudan, and their implication for crustal collision. Geology 22:175–184

Arne D, Brauhart C, King M, Reynolds N (2014) Second phase exploration of Block 62 concession in Sudan, Red Sea Hills. Final Report for Qatar Mining Sudan Co Ltd (unpublished)

Barley ME (1982) Porphyry-style mineralization associated with early calc-alkaline igneous activity, eastern Pilbara, Western Australia. Econ Geol 77:1230–1236

Bejgarn T, Söderlund U, Weihed P, Årebäck H, Ernst RE (2013) Palaeoproterozoic porphyry Cu-Au, intrusion-hosted Au and ultramafic Cu-Ni deposits in the Fennoscandian Shield: temporal constraints using U-Pb geochronology. Lithos 174:236–254

Bierlein FP, Groves DI, Cawood PAC (2009) Metallogeny of accretionary orogens—the connection between lithospheric processes and endowment. Ore Geol Rev 36:282–292

Bodnar RJ (1995) Fluid-inclusion evidence for a magmatic source for metals in porphyry copper deposits. In: Thompson JFH (ed) Magmas, fluids, and ore deposits. Mineralogical Association of Canada short course series 23, p. 139–152

Cottard F, Braux C, Cortial P, Deschamps Y, Elsamani Y, Hottin AM, Younis MO (1986) Les amas sulfurés polymétalliques et les minéralisations aurifères du district d'Ariab (Red Sea Hills, Soudan). Historique de la découverte, cadre géologique et principaux caractèr des gisements. Chroniques Recherches Miniéres 483:19–40

Fitches WRG, Rahamr H, Husseini M, Ries AC, Shackletro NM, Price RC (1983) The late Proterozoic ophiolite of Sol Hamed, NE Sudan. Precambrian Res 19:385–411

Gaál G, Isohanni M (1979) Characteristics of igneous intrusions and various wall rocks in some Precambrian porphyry copper-molybdenum deposits in Pohjanmaa, Finland. Econ Geol 74:1198–1210

Garwin S, Hall R, Watanabe Y (2005) Tectonic setting, geology, and gold and copper mineralization in Cenozoic magmatic arcs of southeast Asia and the west Pacific. In: Hedenquist JW, Thompson JFH, Goldfarb RJ, Richards JP (eds) Society of Economic Geologists, Economic Geology 100th Anniversary Volume, p. 891–930

Goodman S, Williams-Jones AE, Carles P (2005) Structural controls on the Archean Troilus gold–copper deposit, Quebec, Canada. Econ Geol 100:577–582

Groves DI, Vielreicher RM, Goldfarb RJ, Condie KC (2005) Controls on the heterogeneous distribution of mineral deposits through time. Geol Soc Lond Spec Publ 248:71–101

Gustafson LB, Hunt JP (1975) The porphyry copper deposit at El Salvador, Chile. Econ Geol 70:857–912

Halpin JA, Jensen T, McGoldrick P, Meffre S, Berry RF, Everard JL, Calver CR, Thompson J, Goemann K, Whittaker JM (2014) Authigenic monazite and detrital zircon dating from the Proterozoic Rocky Cape Group, Tasmania: Links to the Belt-Purcell Supergroup, North America, Precambrian Research 250:50-67

John DA, Ayuso RA, Barton MD, Blakely RJ, Bodnar RJ, Dilles JH, Gray F, Graybeal FT, Mars JC, McPhee DK, Seal RR, Taylor RD, Vikre PG (2010) Porphyry copper deposit model, chap. B *of* Mineral deposit models for resource assessment: U.S. Geological Survey Scientific Investigations Report 2010–5070–B, 169 p

Johnson PR, Andresen A, Collins AS, Fowler AR, Fritz H, Ghebreab W, Kusky T, Stern RJ (2011) Late cryogenian–ediacaran history of the Arabian–nubian shield: A review of depositional, plutonic, structural, and tectonic events in the closing stages of the northern East African Orogen. J Afr Earth Sci 61:167–232

Kerrich R, Goldfarb RJ, Richards J (2005) Metallogenic provinces in an evolving geodynamic framework. In: Hedenquist JW, Thompson JFH, Goldfarb RJ, Richards JP (eds) Economic geology 100th anniversary volume. Society of Economic Geologists, Littleton, Colorado, pp 1097–1136

Kesler SE, Wilkinson BH (2006) The role of exhumation in the temporal distribution of ore deposits. Econ Geol 101:919–923

Klemenic PM (1985) New geochronological data on volcanic rocks from northeast Sudan and their implication for crustal evolution. Precambrian Res 30:263–276

Klemm D, Klemm R, Murr A (2001) Gold of the pharaohs—6000 years of gold mining in Egypt and Nubia. J Afr Earth Sci 33:643–659

Kröner A, Stern RJ (2005) Pan-African Orogeny, North African Phaerozoic Rift Valley, Encyclopedia of Geology (2004), vol 1. Elsevier, Amsterdam

Kröner A, Greiling R, Reischmann T, Hussein IM, Stern RJ, Durr S, Kruger J, Zimmer M (1987) Pan-African crustal evolution in the Nubian segment of NE Africa. In: Kröner A (Ed) Proterozoic Lithospheric Evolution, American Geophysical Union Geodynamics Series, vol. 17, pp. 235–257

Ludwig KR (2012) User's manual for isoplot—a geochronological toolkit for Microsoft Excel. Berkeley Geochronology Center Special Publication 5, 75p (http://www.bgc.org/isoplot_etc/isoplot/Isoplot3_75-4_15manual.pdf)

Malenda M, Friehauf K, Mathur R (2014) Re-Os isotopic dating of the Mesoproterozoic Haib porphyry copper deposit, southern Namibia. 2014 GSA Annual Meeting in Vancouver, British Columbia (19–22 October 2014) Abstracts Volume, pp. xxx

de Oliveira CG, de Oliveira FB, Schutesky Della Giustina ME, Campos Marques G, Dantas EL, Pimentel MM, Buhn BM (2015) The Chapada Cu–Au deposit, Mara Rosa magmatic arc, central Brazil: constraints on the metallogenesis of a Neoproterozoic large porphyry-type deposit. Ore Geol Rev 72:1–21

Qui Y, Groves DI (1999) Late Archean collision and delamination in the Southwest Yilgarn Block: the driving force for Archean orogenic lode gold mineralization. Econ Geol 94:115–122

Reischmann T, Kröner A (1994) Late Proterozoic island arc volcanics from Gebeit, Red Sea Hills, north-east Sudan. Geolog Rundsch 83:547–562

Richards JR (2009) Postsubduction porphyry Cu–Au and epithermal Au deposits: products of remelting of subduction-modified lithosphere. Geology 37:247–250

Richards JP, Boyce AJ, Pringle MS (2001) Geological evolution of the Escondida area, northern Chile: a model for spatial and temporal localization of porphyry Cu mineralization. Econ Geol 96:271–305

Scott SD (1983) Chemical behavior of sphalerite and arsenopyrite in hydrothermal and metamorphic environments. Mineral Mag 47:427–435

Seedorff E, Dilles JH, Proffett JM Jr, Einaudi MT, Zurcher L, Stavast WJA, Johnson DA, Barton MD (2005) Porphyry deposits—characteristics and origin of hypogene features. In: Hedenquist JW, Thompson JFH, Goldfarb RJ, Richards JP (eds) Society of Economic Geologists, Economic Geology 100th Anniversary Volume, 1905–2005, p. 251–298

Sibson RH (2001) Seismogenic framework for hydrothermal transport and ore deposition: reviews in. Econ Geol 14:25–50

Sillitoe RH (2000) Styles of high-sulphidation gold, silver, and copper mineralization in porphyry and epithermal environments. AusIMM Proc 305:19–34

Sillitoe RH (2010) Porphyry copper systems. Econ Geol 105:3–41

Stacey JS, Kramers JD (1975) Approximation of terrestrial lead isotope evolution by a two-stage model. Earth Planet Sci Lett 26:207–221

Stein HJ, Hannah JL, Zimmerman A, Markey RJ, Sarkar SC, Pal AB (2004) A 2.5 Ga porphyry Cu-Mo-Au deposit at Malanjkhand, central India: implications for Late Archean continental assembly. Precambrian Res 134:189–226

Stern RJ (1994) Arc assembly and continental collision in the Neoproterozoic east African Orogen: implication for the consolidation of Gondwanaland. Annu Rev Earth Planet Sci 22:319–351

Stern RJ (2002) Crustal evolution in the East African Orogen: a neodymium isotopic perspective. J Afr Earth Sci 34:109–117

Sun WD, Liang HY, Ling MX, Zhan MZ, Ding X, Zhang H, Yang XY, Li YL, Ireland TR, Wei QR, Fan WM (2013) The link between reduced porphyry copper deposits and oxidized magmas. Geochim Cosmochim Acta 103:263–275

Vail JR (1985) Pan-African (late Precambrian) tectonic terrains and the reconstruction of the Arabian–Nubian Shield. Geology 13:839–884

Vos IMA, Bierlein FP, Heithersay PS (2007) A crucial role for slab break-off in the generation of world-class mineral deposits: insights from central and eastern Australia. Mineral Deposita 42:515–522

Walshe JL, Heithersay PS, Morrison GW (1995) Toward an understanding of the metallogeny of the Tasman Fold Belt System. Econ Geol 90:1382–1401

Wu C, Huayong C, Hollings P, Xu D, Liang P, Han J, Xiao B, Cai K, Liu Z, Qi Y (2015) Magmatic sequences in the Halasu Cu Belt, NW China: trigger for the Paleozoic porphyry Cu mineralization in the Chinese Altay—East Junggar. Ore Geol Rev 71:373–404

Yakubchuk AS, Shatov VV, Kirwin D, Edwards A, Tomurtogoo O, Badarch G, Buryak VA (2005) Gold and base metal metallogeny of the central Asian orogenic supercollage. In: Hedenquist JW, Thompson JFH, Goldfarb RJ, Richards JP (eds) Society of Economic Geologists, Economic Geology 100th Anniversary Volume, 1905–2005, pp. 1035-1068